

Instability constraints for the electron temperature anisotropy in the slow solar wind. Thermal core vs. suprathermal halo.

M. Lazar,^{1,2} S.M. Shaaban,^{2,3} V. Pierrard,^{4,5} H. Fichtner,¹ S. Poedts²

¹Institut für Theoretische Physik, Lehrstuhl IV: Weltraum- und Astrophysik, Ruhr-Universität Bochum, D-44780 Bochum, Germany, mlazar@tp4.rub.de

²Centre for Mathematical Plasma Astrophysics, Celestijnenlaan 200B, 3001 Leuven, Belgium

³Theoretical Physics Research Group, Physics Dept., Faculty of Science, Mansoura University, 35516, Egypt

⁴Royal Belgian Institute for Space Aeronomy, av. Circulaire 3, B-1180 Brussels, Belgium

⁵Center for Space Radiations, Université Catholique de Louvain, Place Louis Pasteur 3 bte L4.03.08, 1348 Louvain-La-Neuve, Belgium

ABSTRACT

This letter presents the results of an advanced parametrization of the solar wind electron temperature anisotropy and the instabilities resulting from the interplay of the (bi-)Maxwellian core and (bi-)Kappa halo populations in the slow solar wind. A large set of observational data (from the Ulysses, Helios and Cluster missions) is used to parametrize these components and establish their correlations. The instabilities are significantly stimulated in the presence of suprathermals, and the instability thresholds shape the limits of the temperature anisotropy for both the core and halo populations re-stating the incontestable role that the selfgenerated instabilities can play in constraining the electron anisotropy. These results confirm a particular implication of the suprathermal electrons which are less dense but hotter than thermal electrons.

Subject headings: Space plasmas: solar wind – temperature anisotropy – instabilities

1. Observational motivation

The velocity distributions of electrons in the solar wind are well represented by a combination of a Maxwellian core at low-energies and Kappa power-law at higher energies, suggesting the existence of two distinct (but inter-correlated) populations, namely a thermal core and a suprathermal Kappa-distributed halo (*Maksimovic et al.* 2005; *Stverak et al.* 2008; *Pierrard et al.* 2016). An additional strahl component drifting along the magnetic field in antisunward direction can also be observed, but mainly during the energetic events (e.g., fast winds and coronal mass ejections) and mainly at small (less than 1 AU) heliocentric distances (*Maksimovic et al.* 2005). Otherwise the implication of strahls is minimal, and

the electron dynamics is controlled by the interplay of the core and halo populations.

The solar wind electrons exhibit a temperature anisotropy with respect to the (local) magnetic field direction, but the anisotropy does not increase indefinitely as would result from different concurrent processes, such as the fluid-like expansion, magnetic compression, or dissipation (at lower scales) via wave-particle resonances. At large radial distances particle-particle collisions are not efficient and the selfgenerated instabilities may act constraining large deviations from isotropy. The observations have already confirmed this scenario but only for the core components of the solar wind electrons (*Stverak et al.* 2008) and protons (*Hellinger et al.* 2006). To be precise, the instability thresholds predicted by the linear theory for these bi-Maxwellian populations have been found to approach well enough the limits of temperature anisotropy observed in the solar wind.

Here we analyze the implications of the suprathermal electrons which are ubiquitous in the solar wind. Being more tenuous and hotter than the core, suprathermal populations may be sources of free energy for the selfgenerated instabilities (*Viñas et al.* 2010; *Wilson III et al.* 2013), which are expected to grow faster and exhibit lower threshold conditions in the presence of suprathermals (*Shaaban et al.* 2016; *Lazar et al.* 2017). If we refer to the solar wind electrons, the core and halo components cannot exist independently, and their interplay can be inferred from the correlations of different quantities, e.g., temperature anisotropy and (parallel) plasma beta, which are the principal parameters conditioning the instability thresholds. Distinctive descriptions revealing correlations of these two populations are not abundant in the literature. Early studies were limited in characterizing the halo as a remainder after measuring the core (bi-Maxwellian fitting or numerical integration) and extracting from the total distribution (*McComas et al.* 1992; *Phillips et al.* 1995), or by fitting both components with standard bi-Maxwellians (*Pilipp et al.* 1987; *Maksimovic et al.* 1997, 2000). A more accurate description has been provided later with

a dual fitting model combining a bi-Maxwellian core and a bi-Kappa halo (*Maksimovic et al.* 2005; *Stverak et al.* 2008; *Pierrard et al.* 2016). Emphasis has been given to the evolution of these two electron components as a function of heliocentric distance and latitude, mainly from an attempt to understand the origin of suprathermal electrons as well as their implication in the regulation of the energy budget and key processes (like plasma heating and particle acceleration) in the solar wind. The relative halo to core density is roughly constant over heliocentric distance with the halo representing 4 % of the total electron density (*McComas et al.* 1992), but out of the ecliptic it shows an increasing tendency to reach values of 10 to 30 % of the total density (*Maksimovic et al.* 2005) and a steep radial gradient (*Maksimovic et al.* 2000). For the halo (subscript h) to core (subscript c) temperature contrast *Maksimovic et al.* (2000) have found a modest variation with the solar wind bulk speed, i.e., mean values $T_h/T_c \simeq 13.57$ in the slow wind ($V_{SW} < 600$ km/s), and $T_h/T_c \simeq 23.38$ in the fast wind ($V_{SW} > 600$ km/s), although their bi-Maxwellian representation for the halo component cannot reproduce details of the distribution which may be important in the analysis of the temperature anisotropy instabilities. These authors have also studied the so-called suprathermal strength $S \equiv n_h T_h / n_c T_c$ (the ratio of the halo to core kinetic pressures), which is actually giving the correlation of the halo and core plasma beta parameters, i.e., $S = \beta_h / \beta_c$ (where $\beta = 8\pi n k_B T / B_0^2$ is the ratio of the kinetic and magnetic field pressures), and found average values higher in the fast ($S \simeq 0.79$) than the slow ($S \simeq 0.39$) wind.

The temperature anisotropies of the electron core and halo populations have been measured by *Stverak et al.* (2008) for more than 120.000 events detected in the ecliptic by three spacecraft (Helios, Cluster and Ulysses) and covering the radial distances from the Sun from 0.3 up to 4 AU. Parallel and perpendicular temperatures ($T_{\parallel, \perp}$, with respect to the local magnetic field) are determined from fitting the observed velocity distribution (after instrumental corrections) with a gyrotropic dual model that combines a bi-Maxwellian

core with a bi-Kappa halo. Limits of the temperature anisotropy ($A = T_{\perp}/T_{\parallel}$) observed in the solar wind have been compared with the instability thresholds predicted by the linear kinetic theory for a bi-Maxwellian distributed plasma, i.e., the whistler instability driven by an excess of perpendicular temperature $T_{\perp} > T_{\parallel}$, and the firehose instability driven by $T_{\parallel} > T_{\perp}$. Good agreements between these instability thresholds and the limits of the temperature anisotropy are found only for the electron core population in the slow winds (i.e., with a bulk speed $V < 500$ km/s). The halo component shows significant departures from the anisotropy thresholds especially for the firehose instability. Even stronger differences are obtained for both the core and halo populations in the fast wind ($V > 600$ km/s), but our analysis in the present paper focuses on the slow wind conditions. The disagreement obtained for the halo component must have an immediate explanation (also suggested by the authors) in the facts that (i) the theoretical model used in the linear prediction of the instabilities (bi-Maxwellian) is different than that used to reproduce the observed halo data (bi-Kappa), and (ii) theoretical predictions for the halo component neglect completely the possible effect of the core. In this letter we present the results of an advanced stability analysis, intended to decode the interplay of the electron core and halo populations from a realistic parametrization in accord with the fitting model. The core-halo correlations between physical quantities, e.g., relative densities, anisotropies and (parallel) plasma betas are identified from the observations in section 2. We then derive the instability thresholds for the whistler and firehose instabilities and compare with the limits of temperature anisotropy observed in the solar wind (section 3). The results are discussed in section 4.

2. Core-halo correlations

Pierrard et al. (2016) have used the same set of electron data invoked by *Stverak*

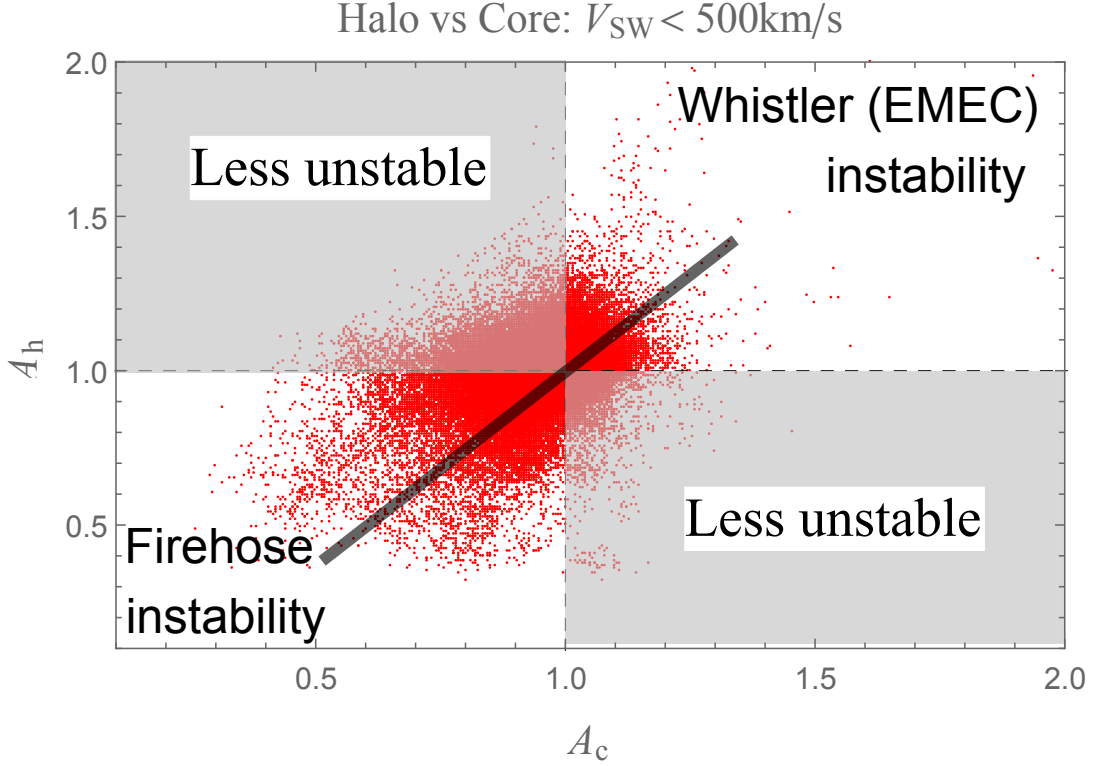


Fig. 1.— Temperature anisotropies A_h vs. A_c in slow winds ($V_{\text{SW}} < 500$ km/s).

et al. (2008) to investigate the solar wind electron temperature and its anisotropy making a distinction between the core and halo components, and also suggesting a series of correlations which we invoke in the present analysis. Thus, the halo temperature shows a clear variation with the power-index κ , which quantifies the presence of suprathermals in a bi-Kappa distribution, and *Lazar et al.* (2017) have found for this dependence

$$T_h = T_M \kappa / (\kappa - 1.5), \quad (1)$$

where T_M is a (Maxwellian) limit value. This law is in perfect agreement with the radial evolution of the halo temperature that increases while the power-index κ increases.

Plots correlating the temperature anisotropies of the core and halo components are provided in Fig. 5 from *Pierrard et al.* (2016), where the data points show a prevailing

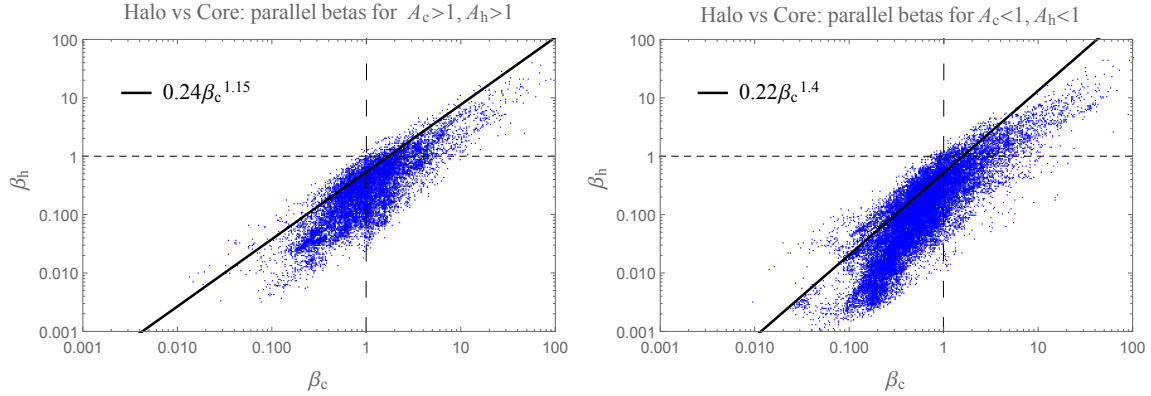


Fig. 2.— Parallel plasma betas $\beta_{h,\parallel}$ vs. $\beta_{c,\parallel}$ in slow winds ($V_{\text{SW}} < 500$ km/s), for $A_{c,h} > 1$ (top) and $A_{c,h} < 1$ (bottom).

disposition to align along a linear regression $A_h = A_c$, suggesting directly correlated anisotropies. Here in Fig. 1 we rebuild such a plot of A_h vs. A_c , but with the full set of data. Linear regression $A_h = A_c$ is shown with a solid line, and the isotropic conditions $A_h = 1$ or $A_c = 1$ are drawn with dashed lines. Dominant appear to be the states with $A_c < 1$, and among these most abundant are the symmetric states with both $A_h < 1$ and $A_c < 1$, which are the most unstable against the excitation of the firehose instability (FHI). The opposite quadrant contains states with both $A_h > 1$ and $A_c > 1$, which are the most unstable to the excitation of the electromagnetic electron cyclotron (EMEC) instability also known as the whistler instability (WI). In the other two quadrants, the core and halo exhibit opposite (or anticorrelated) anisotropies, i.e., $A_h > 1$ and $A_c < 1$ (top), or $A_h < 1$ and $A_c > 1$ (bottom). These plasma states are less unstable (a detailed study of the interplay of the core and halo instabilities will be presented elsewhere), and the resulting instabilities will not evolve fast enough to be efficient in constraining the temperature anisotropy of the solar wind electrons. Instead, the WI is highly stimulated when both $A_{c,h} > 1$, and the FHI when both $A_{c,h} < 1$.

In Figure 2 we display $\beta_{h,\parallel}$ vs. $\beta_{c,\parallel}$ for each of these two cases of interest here, and the

best linear fitting (log-log scales) plotted over with solid lines provides $\beta_{h,\parallel} = 0.24\beta_{c,\parallel}^{1.15}$ for $A_{c,h} > 1$ (top panel), and $\beta_{h,\parallel} = 0.22\beta_{c,\parallel}^{1.4}$ for $A_{c,h} < 1$ (bottom panel). Other key parameters in the dispersion/stability analysis are the relative density numbers of electrons in the core $\eta_c = n_c/n_0$ and halo $\eta_h = n_h/n_0$ components ($n_0 = n_{\text{total}}$ is the total density number), which are evaluated using the observational data in Table 1 from *Pierrard et al. (2016)*. We find the following mean values $\eta_c = 0.966$ for the core, and $\eta_h = 0.034$ for the halo, implying for the halo-core number density contrast $\eta = n_h/n_c = 0.035$, almost the same with that obtained by *McComas et al. (1992)* in similar conditions in the ecliptic.

3. Instability thresholds vs. observations

The stability analysis may invoke the electromagnetic cyclotron modes, which are particularly important in establishing resonant interactions with magnetized plasma particles, and constraining their temperature anisotropy. The fastest growing mode driven by the electrons with $A > 1$ is the parallel whistler instability (also known as the electromagnetic electron cyclotron mode) with growth rates higher than the other oblique modes including the propagating whistlers (*Kennel and Petschek 1966*) and the non-propagating mirror instability (*Gary and Karimabadi 2006*) which can be ignored (*Stverak et al. 2008*). High-frequency whistlers are right-handed polarized modes which do not interact with protons and are described by the dispersion relation

$$\begin{aligned} \tilde{k}^2 = \frac{1}{\eta} & \left[A_c - 1 + \frac{A_c(\tilde{\omega} - 1) + 1}{\tilde{k}\sqrt{\eta\beta_{c,\parallel}}} Z_M \left(\frac{\tilde{\omega} - 1}{\tilde{k}\sqrt{\eta\beta_{c,\parallel}}} \right) \right] \\ & + A_h - 1 + \frac{A_h(\tilde{\omega} - 1) + 1}{\tilde{k}\sqrt{\beta_{h,\parallel}^M}} Z_\kappa \left(\frac{\tilde{\omega} - 1}{\tilde{k}\sqrt{\beta_{h,\parallel}^M}} \right) \end{aligned} \quad (2)$$

where $\tilde{\omega} = \omega/\Omega = \tilde{\omega}_r + i\tilde{\gamma}$ (including the wave-frequency $\tilde{\omega}_r$ and the growth-rate $\tilde{\gamma}$) and wave-number $\tilde{k} = kc/\omega_{e,h}$ are normalized by, respectively, the electron gyro-frequency

$\Omega = |\Omega_e|$ and the halo plasma frequency $\omega_{e,h}$, and Z_M and Z_κ are the plasma dispersion functions for the Maxwellian and Kappa distributed plasmas (see for instance the definitions in *Shaaban et al. (2016)*). $\beta_{h,\parallel}^M$ corresponds to the Maxwellian (limit) temperature in Eq. 1, $\beta_{h,\parallel} = \beta_{h,\parallel}^M \kappa / (\kappa - 1.5)$. In parallel direction the low-frequency electron FHI is a left-handed polarized mode described by

$$\begin{aligned} \tilde{k}^2 = & \eta_c \mu \left[A_c - 1 + \frac{A_c (\tilde{\omega} + \mu) - \mu}{\tilde{k} \sqrt{\mu \beta_{c,\parallel}} / \eta_c} Z_M \left(\frac{\tilde{\omega} + \mu}{\tilde{k} \sqrt{\mu \beta_{c,\parallel}} / \eta_c} \right) \right] \\ & + \eta_h \mu \left[A_h - 1 + \frac{A_h (\tilde{\omega} + \mu) - \mu}{\tilde{k} \sqrt{\mu \beta_{h,\parallel}^M} / \eta_h} Z_\kappa \left(\frac{\tilde{\omega} + \mu}{\tilde{k} \sqrt{\mu \beta_{h,\parallel}^M} / \eta_h} \right) \right] \\ & + \frac{\tilde{\omega}}{\tilde{k} \beta_{p,\parallel}} Z_M \left(\frac{\tilde{\omega} - 1}{\tilde{k} \sqrt{\beta_{p,\parallel}}} \right), \end{aligned} \quad (3)$$

where the frequency $\tilde{\omega} = \omega / \Omega_p = \tilde{\omega}_r + i\tilde{\gamma}$ and wave-number $\tilde{k} = kc / \omega_p$ are normalized by, respectively, the proton gyro-frequency Ω_p and proton plasma frequency ω_p . The influence of protons ($\mu = m_p / m_e = 1836$) is minimized assuming isotropic and of finite temperature, with $\beta_{p,\parallel} = \beta_{c,\parallel} / 2$.

We use these dispersion relations and the parametrization established in previous section to derive the temperature anisotropy thresholds as curves of constant (maximum) growth rates $\tilde{\gamma}_m = 10^{-3}, 10^{-2}$. The anisotropy curves are described as inverse correlation laws of the parallel plasma beta, i.e., $A = 1 + a / \beta_{\parallel}^b$, and values obtained for the fitting parameters a and b are tabulated in Tables 1 and 2. The instability conditions are determined for two values of the power-index $\kappa = 3$ and 8, representative for sufficiently many events with, respectively, the lowest and highest κ -values from our data set. In Figures 3 and 4 thresholds of WI and FHI are contrasted with the temperature anisotropy measured in the solar wind, for the thermal (Maxwellian) core (Figure 3) and for the suprathermal (Kappa) halo (Figure 4). The distribution of observational data providing A vs. β_{\parallel} is shown with histogram contours to count the events.

Table 1: Parameters a , b for the core anisotropy thresholds.

Wave	WI				FHI			
$\tilde{\gamma}_m$	10^{-3}		10^{-2}		10^{-3}		10^{-2}	
	a	b	a	b	$-a$	b	$-a$	b
$\kappa = 3$	0.18	0.59	0.34	0.53	1.60	1.10	1.60	1.10
$\kappa = 8$	0.16	0.60	0.34	0.53	1.55	1.11	1.55	1.10
bi-Max.	0.25	0.50	0.43	0.47	1.76	1.04	1.70	0.99

4. Discussion and conclusion

The in-situ measurements of the velocity distributions of electrons in space plasmas (e.g., the solar wind and planetary magnetospheres) indicate the existence of two distinct but intercorrelated components, namely, a thermal core at low energies and a less dense but more energetic suprathermal halo. We have derived the temperature anisotropy thresholds of the whistler and firehose instabilities from the interplay of the core and halo populations, which are parametrized on the basis of a large set of observational data from Ulysses, Helios and Cluster missions. The correlations established between the core and halo parameters which determine the growth of instability (i.e., temperature anisotropy, parallel plasma beta and relative number density) enabled us to derive the instability thresholds function of either the core or halo parameters. Comparing with the observations, we find that the instability thresholds (solid and dashed lines) shape the limits of the temperature anisotropy for both the core (Figures 3) and halo (Figures 4) populations. By these results linear stability predicts for the first time that the selfgenerated instabilities may regulate the anisotropic halo component. The instability constraints appear to be markedly strengthened by the cumulative effect of these two components as the new refined thresholds are lower than those predicted for a bi-Maxwellian core (dotted lines) by neglecting the influence of the suprathermal (bi-Kappa) halo. We are aware of the fact that

Table 2: Parameters a , b for the halo anisotropy thresholds.

Wave	WI				FHI			
$\tilde{\gamma}_m$	10^{-3}		10^{-2}		10^{-3}		10^{-2}	
	a	b	a	b	$-a$	b	$-a$	b
$\kappa = 3$	0.09	0.513	0.17	0.45	0.48	0.79	0.49	0.78
$\kappa = 8$	0.08	0.516	0.17	0.45	0.47	0.79	0.47	0.79

for bi-Maxwellian electrons with $A < 1$ the nonpropagating FHI develops obliquely to the magnetic field and faster (with higher growth-rates and lower thresholds) than the parallel FHI (*Li and Habbal 2000; Camporeale and Burgess 2008*). Indicated by the observations, the new Maxwellian-Kappa model invoked here is more complex and make the analysis of the oblique modes less straightforward. However, an extended investigation on the full wave-vector spectrum is strongly motivated by the the results reported in the present paper and will make the object of our next studies.

M.L. acknowledges support from the Katholieke Universiteit Leuven, Ruhr-University Bochum and Alexander von Humboldt Foundation. These results were obtained in the framework of the projects SCHL 201/35-1 (DFG–German Research Foundation), G0A2316N (FWO–Vlaanderen), GOA/2015-014 (KU Leuven), and C 90347 (ESA Prodex). This research has been funded by the Interuniversity Attraction Poles Programme initiated by the Belgian Science Policy Office (IAP P7/08 CHARM). S.M.S. would like to thank the Egyptian Ministry of Higher Education for supporting his research activities. Thanks are due to Š. Štverák for providing the observational data.

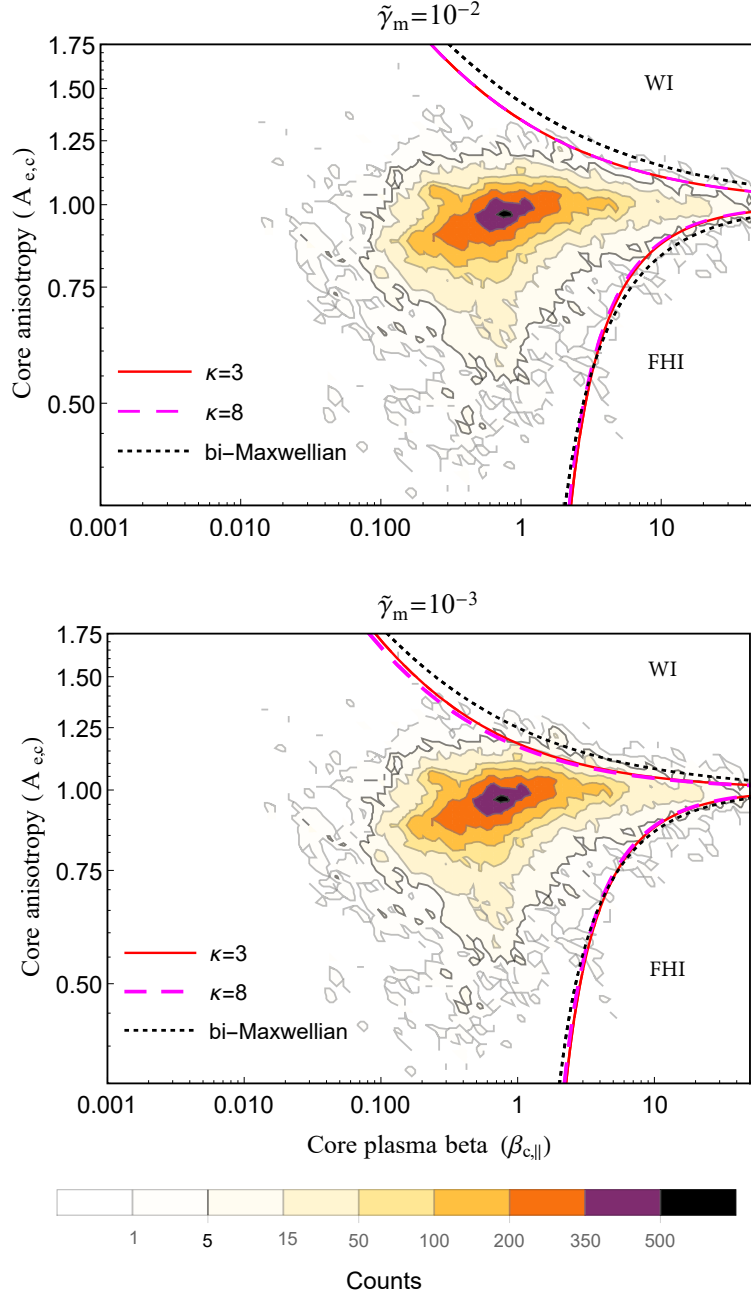


Fig. 3.— Comparison of the instability (WI and FHI) thresholds for $\tilde{\gamma}_m = 10^{-3}$ and 10^{-2} , with the core temperature anisotropy displayed using a histogram data (counts in color bar).

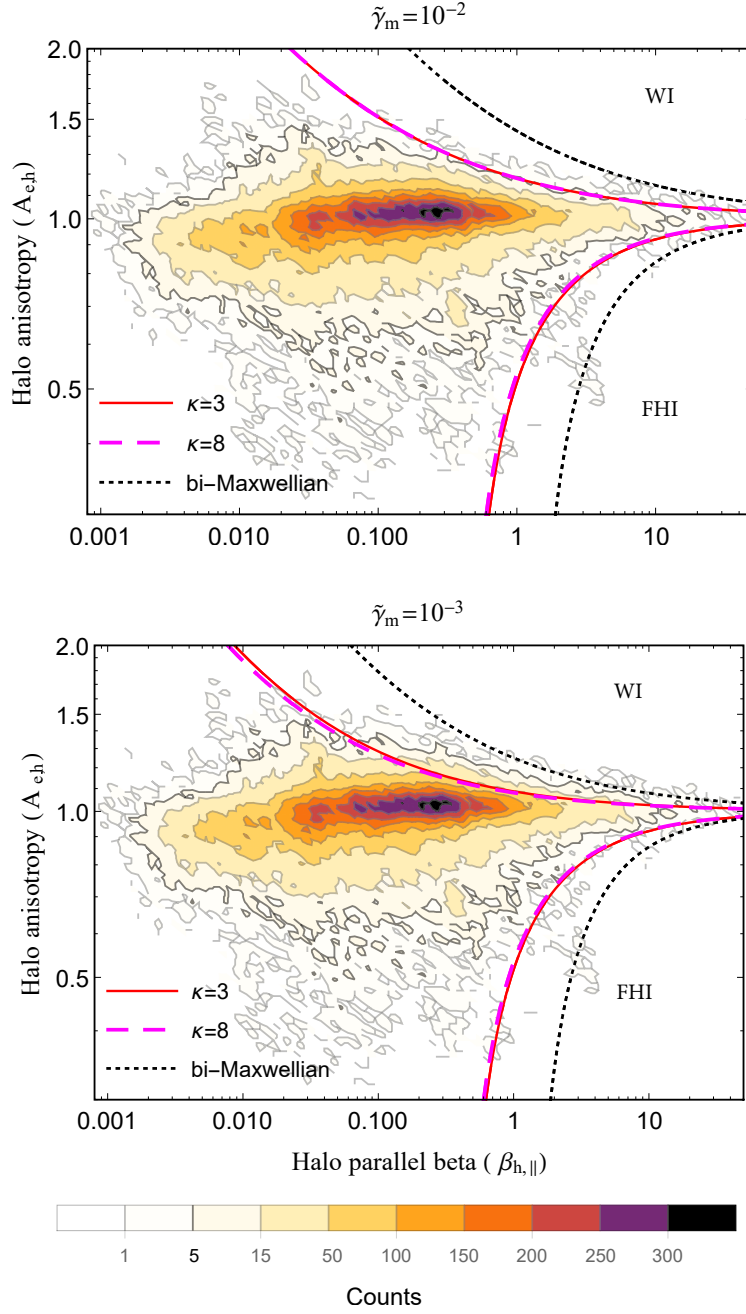


Fig. 4.— Comparison of the instability (WI and FHI) thresholds for $\tilde{\gamma}_m = 10^{-3}$ and 10^{-2} , with the halo temperature anisotropy displayed using a histogram data (counts in color bar).

REFERENCES

- Camporeale, E., and Burgess, D. 2008, Electron firehose instability: Kinetic linear theory and two-dimensional particle-in-cell simulations, *J. Geophys. Res.*, 113, A07107
- Gary P., H. Karimabadi (2006), Linear theory of electron temperature anisotropy instabilities: Whistler, mirror, and Weibel, *J. Geophys. Res.*, 111, A11224.
- Kennel C. F., H. E. Petschek (1966), Limit on stably trapped particle fluxes, *J. Geophys. Res.*, 71, 1.
- Hellinger, P., Trávníček, P., Kasper, J. C., & Lazarus, A. J. 2006, *Geophys. Res. Lett.*, 33, L09101.
- Lazar, M., Schlickeiser, R., Poedts, S.: 2012, Suprathermal Particle Populations in the Solar Wind and Corona, in Exploring the Solar Wind, ed. M. Lazar (InTech), Ch. 11, <http://www.intechopen.com/books/exploring-the-solar-wind>
- Lazar, M., V. Pierrard, S.M. Shaaban, H. Fichtner, and S. Poedts (2017), Dual Maxwellian-Kappa modelling of the solar wind electrons: new clues on the temperature of Kappa populations, *Astron. Astrophys.* (submitted).
- Li, X., and Habbal, S. R. 2000, Electron kinetic firehose instability, *J. Geophys. Res.*, 105, 27377
- Maksimovic M., I. Zouganelis, J.-Y. Chaufray, K. Issautier, E. E. Scime, J. E. Littleton, E. Marsch, D. J. McComas, C. Salem, R. P. Lin, H. Elliott (2005), Radial evolution of the electron distribution functions in the fast solar wind between 0.3 and 1.5 AU, *J. Geophys. Res.*, 110, A09104.
- Maksimovic M., S.P. Gary, and R.M. Skoug (1997), Solar wind electron suprathermal

- strength and temperature gradients: Ulysses observations, *J. Geophys. Res.*, *105*, 18,337.
- Maksimovic M., V. Pierrard, and P. Riley (1997), Ulysses electron distributions fitted with Kappa functions, *Geophys. Res. Lett.*, *24*, 1151.
- McComas D. J., S. J. Bame, W. C. Feldman, J. T. Gosling, J. L. Phillips (1992), Solar wind halo electrons from 1-4 AU, *Geophys. Res. Lett.*, *19*, 2951.
- Pierrard V., M. Lazar (2010), Kappa Distributions: Theory and Applications in Space Plasmas, *Solar Phys.*, *267*, 153.
- Pierrard V., M. Lazar, S. Poedts, S. Stverak, M. Maksimovic, P.M. Travnicek (2016), The Electron Temperature and Anisotropy in the Solar Wind. Comparison of the Core and Halo Populations, *Solar Phys.*, *291*, 2165.
- Pilipp W. G., K.-H. Muehlhaeuser, H. Miggenrieder, M.D. Montgomery, H. Rosenbauer, (1987), Characteristics of electron velocity distribution functions in the solar wind derived from the HELIOS plasma experiment *J. Geophys. Res.*, *92*, 1075.
- Phillips J. L., S. J. Bame, S. P. Gary, J. T. Gosling, E. E. Scime, R. J. Forsyth, (1995), Radial and Meridional Trends in Solar Wind Thermal Electron Temperature and Anisotropy: ULYSSES”, *Space Sci. Rev.*, *72*, 109.
- Shaaban S. M., M. Lazar, S. Poedts, S., A. Elhanbaly (2016), *J. Geophys. Res.: Space Physics*, *121*, 6031, 2016JA022587
- Stverak, S., P. Travnicek, M. Maksimovic, E. Marsch, A.N. Fazakerley, E.E. Scime (2008), Electron temperature anisotropy constraints in the solar wind, *J. Geophys. Res.*, *113*, A03103

Viñas A. F., C. Gurgiolo, T. Nieves-Chinchilla, S. P. Gary, M. L. Goldstein (2010), Whistler waves driven by anisotropic strahl velocity distributions: Cluster observations, *AIP Conf. Proceedings*, 1216, 265.

Wilson III L. B., A. Koval, A. Szabo, A. Breneman, C. A. Cattell, K. Goetz, P. J. Kellogg, K. Kersten, J. C. Kasper, B. A. Maruca, M. Pulupa (2013), Electromagnetic waves and electron anisotropies downstream of supercritical interplanetary shocks, *J. Geophys. Res.: Space Physics*, 118, 5.